Hindawi
Advances in Civil Engineering
Volume 2021, Article ID 6672430, 12 pages
https://doi.org/10.1155/2021/6672430

*Research Article*

# Experimental Study on Electric Resistivity Characteristics of Compacted Loess under Different Loads and Drying-Wetting Cycles

**Yu Zhou**,[1,2] **Guoyu Li**,[1,2] **Wei Ma**,[1,2] **Dun Chen**,[1] **Fei Wang**,[3] **Yuncheng Mao**,[4] **Qingsong Du**,[1,2] **Jun Zhang**,[1,2] **and Liyun Tang**[5]

[1]*Da Xing'anling Observation and Research Station of Frozen-ground Engineering and Environment, State Key Laboratory of Frozen Soil Engineering, Northwest Institute of Eco-Environment and Resources, Chinese Academy of Sciences, Jagdaqi 165000, Heilongjiang, China*
[2]*College of Resources and Environment, University of Chinese Academy of Sciences, Beijing 100049, China*
[3]*Faculty of Civil Engineering and Mechanics, Jiangsu University, Zhenjiang 212013, China*
[4]*College of Civil Engineering, Northwest Minzu University, Lanzhou 730000, China*
[5]*College of Architecture and Civil Engineering, Xi'an University of Science and Technology, Xi'an 710054, China*

Correspondence should be addressed to Guoyu Li; guoyuli@lzb.ac.cn

Received 16 December 2020; Revised 10 January 2021; Accepted 11 January 2021; Published 29 January 2021

Academic Editor: Song-He Wang



Densely compacted loess foundations of many man-made infrastructures are often exposed to various loads and extreme weathering processes (e.g., drying-wetting cycles), which significantly deteriorate their mechanical properties. Traditional methods applied to characterize soil engineering properties are primarily based on visual inspections, point sensors, or destructive approaches, the results of which often have relatively high costs and cannot provide large-area coverage. The electrical resistivity method is a reasonable alternative that provides a nondestructive, sensitive, and continuous evaluation of the soil physical properties. Thus, the relationships between electrical resistivity and soil strength should be understood, particularly for scenarios in which soils undergo significant loads and cycles of drying and wetting. In this study, a suite of laboratory tests simulating loads (consolidation tests, unconfined compression tests, and uniaxial cyclic unloading-reloading tests) and seasonal field conditions (drying-wetting cycle tests) were conducted to quantitatively assess their deterioration effects on the geophysical and geotechnical properties of compacted loess. The experimental results indicated that electric resistivity decreases with the increase in stress and then approaches a stable value after the stress becomes 200 kPa. During the uniaxial compression process, the electric resistivity corresponds to both the stress and strain of loess in real-time. The electrical resistivity of loess reflects plastic damage under uniaxial unloading-reloading tests, but it is deficient in representing the dissipated energy of loess. The electrical resistivity of loess samples increases as the number of drying-wetting cycles increases but decreases with increasing cycle numbers after stabilization under consolidation load. The electrical resistivity can effectively characterize the mechanical and deformation characteristics of loess samples under loads and drying-wetting cycles, exhibiting a certain potential for long-term monitoring of soil engineering properties.

## 1. Introduction

Loess is a loose aeolian deposit of yellowish silt-sized dust and is generally found in arid and semiarid regions [1, 2]. In China, approximately 6.8% of the land surface is occupied by loess with a total area of approximately 640,000 $km^2$ [3]. Loess deposits are known to be characterized by low density, high porosity, and high collapsibility when they become wet; however, these properties can be improved by dense compaction, prewetting, or chemical stabilization in engineering practice [4, 5]. Therefore, loess has been extensively used as a cheap filling material or foundation soil

in various man-made infrastructures such as buildings, highways, railways, airfields, and hydroengineering projects.

However, the engineering stability of loess is directly affected by many factors, such as the drying-wetting (DW) cycles, traffic load, and seismic activity. In the context of global climate change, extreme weather has become more frequent in many regions, and soils experience significant amounts of water loss and increase and considerable volumetric contraction and expansion under such conditions [6]. Before and after DW cycles, the size, shape, and arrangement of loess particles vary in different degrees. The proportion and average diameter of macropores in the loess particles increase with the increase in the number of DW cycles and eventually result in loess cracking [7, 8], accompanied by a dramatic decrease in the mechanical strength, such as unconfined compressive strength (UCS) and shear strength [9, 10]. In addition, repeated traffic loads strongly affect the long-term performance of subgrades. When a traffic load is applied to the soil subgrade, the stress fields and, thus, physical parameters such as moisture content, pore water pressure, and compactness change accordingly, which results in large and differential settlements, significantly affecting the pavement quality and highway capacity [11, 12]. Therefore, reliable and cost-effective systems are required to monitor the conditions of these engineering parameters and directly maintain the most vulnerable parts of the road network.

Traditionally, field-scale inspections of soil engineering properties commonly utilize field observations and measurements on soil surfaces that require surveyors to walk along the entire structure, such as slope and embankment [13–15], in-situ monitoring techniques such as piezometers and clinometers [16, 17], and destructive techniques such as excavation and drill-holes [18–20]. However, direct observation and monitoring with these methods remain expensive from both human and equipment resource perspectives, and the results are based on several single-point values, which may be unreliable and incomplete and, more importantly, may disturb the original soil pattern, resulting in less accurate evaluations. In addition, remote-sensing-based methods, such as Interferometric Synthetic Aperture Radar (InSAR) [21], photogrammetry using unmanned aerial vehicles [22], and Light Detection and Ranging (LiDAR) [23], can be used to regularly monitor ground movement, but these surveys can only provide topographical information; therefore, they cannot provide real-time monitoring and early warning for structural failure. Thus, a reliable real-time monitoring method is required to identify changes in the internal conditions that precede failure.

The electrical resistivity of soil is known to be a sensitive reflection of many soil properties that are associated with the nature of soil composition (mineralogy, fabric, and particle size distribution), structure (porosity, tortuosity, pore size distribution, and connectivity), water content, temperature, etc. [24–31]. Furthermore, these parameters determine the physical and mechanical properties of soil, which makes it possible to evaluate the engineering properties of soil using electrical resistivity. Various studies investigated the relationship between electrical resistivity and the physical and mechanical properties of soil. For example, Munoz-Castelblanco et al. [32], Seladji et al. [33], and Kibria and Hossain [34] observed that electrical resistivity is related to a variety of hydraulic characteristics of soil, such as water content, saturation, pore water salinity, bulk density, and pore structure. Rinaldi and Cuesta [35] and Liu et al. [36] studied the effect of different compaction degrees on electrical resistivity and attempted to evaluate the degree of soil compaction using electrical resistivity. Long et al. [37] compared and analyzed the relationship between soil resistivity and basic engineering properties at fifteen marine clay sites and indicated that electrical resistivity is negatively correlated with pore water salinity, clay content, plasticity index, and shear strength. Although an increasing number of studies use electrical resistivity to characterize the physical and mechanical properties of soil, the direct application of electrical resistivity methods to monitor engineering stability is still rare. This is primarily because of the uncertainty of soil electrical resistivity affected by loads, DW cycles, etc., after the construction of engineering.

Owing to the load and environmental changes after the engineering works, the relationship between soil strength and electrical resistivity when subjected to load and WD cycles must be understood to evaluate the possibility of long-term monitoring engineering stability based on electrical resistivity method. Therefore, a suite of laboratory tests simulating loads (consolidation tests, unconfined compression tests, and uniaxial cyclic unloading-reloading tests) and seasonal field conditions (DW cycle tests) were conducted to resolve the effects of loads and DW cycles on geotechnical and geophysical properties, which are essential for the success of a long-term monitoring system of engineering stability based on electrical resistivity tomography.

## 2. Materials and Methods

*2.1. The Experimental Soil and Sample Preparation.* The loess used in this investigation, collected from Yongdeng county (36°35′49.64″N, 103°22′45.22″E), Gansu Province, Northwestern China, was extensively used as a primary road embankment fill when the National Lianyungang–Horgos Highway (G30) in Gansu Province was built. According to the Chinese engineering geological zoning map of collapsible loess [38], the sampling site is located in a strongly collapsible loess area with the collapsible grade III or IV. The fundamental properties such as the grain size distribution, specific gravity, plastic and liquid limits, optimum water content, maximum dry density, and soluble salt content of this testing soil are summarized in Figure 1 and Table 1.

After collection from the field, the soil was air-dried naturally, crushed, and sieved using a 2 mm mesh sieve in the laboratory. Sieved loess particles were evenly mixed with an appropriate amount of distilled water to attain the optimum water content of 13%. Subsequently, the set of wet aggregates was stored in a sealed plastic bag for 24 h to homogenize the water content in the soil volume. Then, the soil was placed in a cylindrical steel mould and densely compacted to two types of cylindrical soil samples of

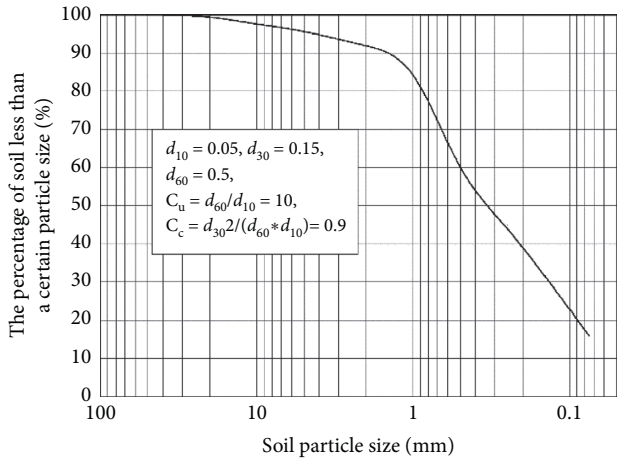


Figure 1: Grain size distribution curve of soil.

Table 1: Basic physical properties of loess sample.

| Parameters | Value |
|---|---|
| Specific gravity Gs | 2.70 |
| Maximum dry density $\rho_{dmax}$ (g/cm$^3$) | 1.912 |
| Optimum moisture content $\omega_{opt}$ (%) | 13.0 |
| Liquid limit $W_L$ (%) | 26.29 |
| Plastic limit $W_P$ (%) | 18.24 |
| Plasticity index $P_I$ (%) | 8.05 |
| Coefficient of collapsibility $\delta_s$ | 0.063–0.108 |
| Soluble salt content (%) | 0.8 |

different sizes with a density of 1.81 g/cm$^3$ close to the Proctor maximum. The first type of loess samples of 61.8 mm diameter and 20 mm height was subjected to consolidation tests, while the second type of loess samples of 61.8 mm diameter and 125 mm height was used to conduct uniaxial compression and uniaxial cyclic unloading-reloading tests. After sample preparation, the individual soil specimen was wrapped with plastic films and placed in a foam box exposed to room temperature (20°C) in a closed system without moisture evaporation.

*2.2. Apparatus.* In this study, unconfined compression and uniaxial unloading-reloading tests were performed in a developed triaxial apparatus, which could accommodate a specimen of 61.8 mm diameter and 125 mm height (Figure 2). A pair of circular electrodes of 40 mm in diameter and 0.05 mm thick, fabricated from copper foil, were attached to the bottom surface of the upper porous stone and the top surface of the lower porous stone using insulating glue. The circular electrodes were connected to an inductance-capacitance-resistance (LCR) digital electric bridge using fine electric wires packaged with insulated skin to measure the electrical impedance of the loess samples. The samples and two pieces of ring-shaped filter paper (40 mm inner diameter and 61.8 mm outer diameter) were sandwiched between the upper and lower porous stones attached to the electrodes.

The consolidation tests were performed using a developed consolidation apparatus [39, 40] (Figure 3). The development of the electrodes, porous stone, and ring-shaped filter paper was similar to that of the developed triaxial apparatus. To eliminate the effect of the metal chamber on resistivity measurement, the soil sample was sheathed using an insulating cutting ring fabricated from high-strength nylon material. The outside of the insulating cutting ring was a special rigid metal ring to prevent lateral deformation of the soil sample. The vertical compression strain $\varepsilon_{si}$ in this study is given by the following formula:

$$\varepsilon_{si} = \frac{h_0 - h_i}{h_0} \times 100\%, \quad (1)$$

where $h_0$ is the initial height of specimen, $h_i$ is the stabilized height at a given load, and the $s$ means the one-dimensional compression test.

The LCR digital bridge TH2810D was adopted to measure the electrical resistivity of the samples. Because the soil resistivity is significantly affected by external environmental factors [41], a series of measures were performed to obtain the soil resistivity as accurately as possible: (i) graphite was evenly applied to both surface ends of the loess sample; (ii) the digital bridge was calibrated before each test, and the measured electricity resistivity was corrected for temperature as suggested by Zha et al. [42]; (iii) to ensure sufficient contact between the sample and the electrode, a 1 kPa prepressure was applied before all tests, and then the stress-strain returned to zero. An AC frequency of 50 Hz was used in the study, and the resistivity values were calculated using

$$\rho = \frac{|Z|S}{L}, \quad (2)$$

where $\rho$ is the soil electrical resistivity (Ω·m), $|Z|$ is the impedance mode (Ω) measured using the LCR digital bridge, $S$ is the circular electrode area (m$^2$), and $L$ is the distance between the two circular electrodes (m).

### 2.3. Test Procedures

*2.3.1. Consolidation Tests.* Using the developed consolidation apparatus, consolidation tests were performed on loess specimens to assess their deformation and electrical resistivity behavior at the optimum water content at loads of 12.5, 25, 50, 100, 200, 400, 800, and 1600 kPa [43]. The compression deformation was assumed to be stabilized at this load when the measured vertical settlement for a particular load was not greater than 0.01 mm/h, and a new load was applied. To prevent excessive evaporation, which could cause erroneous results, the soil specimens were covered with cotton gauze during these tests. The LCR digital bridge synchronously monitored the electrical resistivity of loess samples during the consolidation tests and collected data every 2 s.

*2.3.2. Unconfined Compression and Uniaxial Cyclic Unloading-Reloading Tests.* Unconfined compression tests were performed using the developed triaxial apparatus at a vertical strain rate of 1.25 mm/min according to the testing

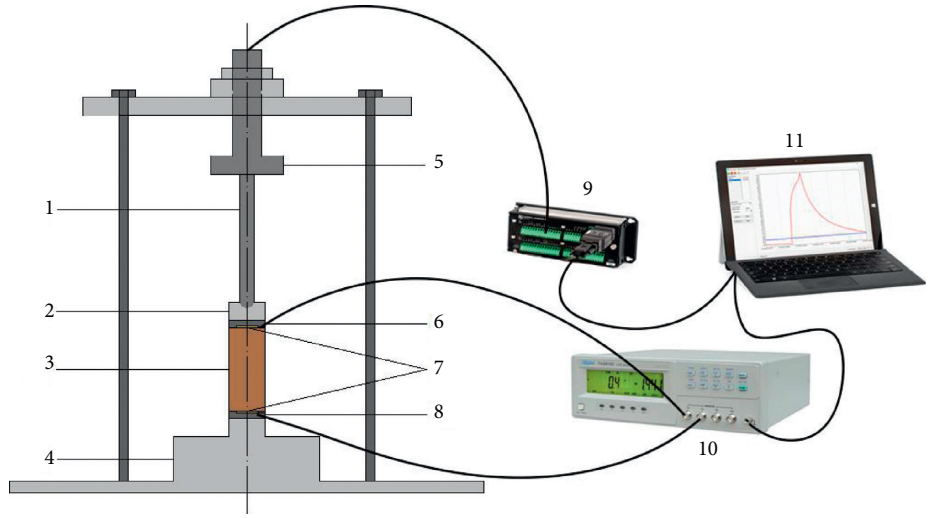


Figure 2: Schematic diagram of the developed triaxial apparatus. Notes: 1: vertical loading unit; 2: loading piston; 3: soil sample; 4: pedestal; 5: pressure sensor; 6: upper porous stone; 7: electrodes; 8: lower porous stone; 9: dara logger; 10: LCR digital electric bridge; 11: computer.

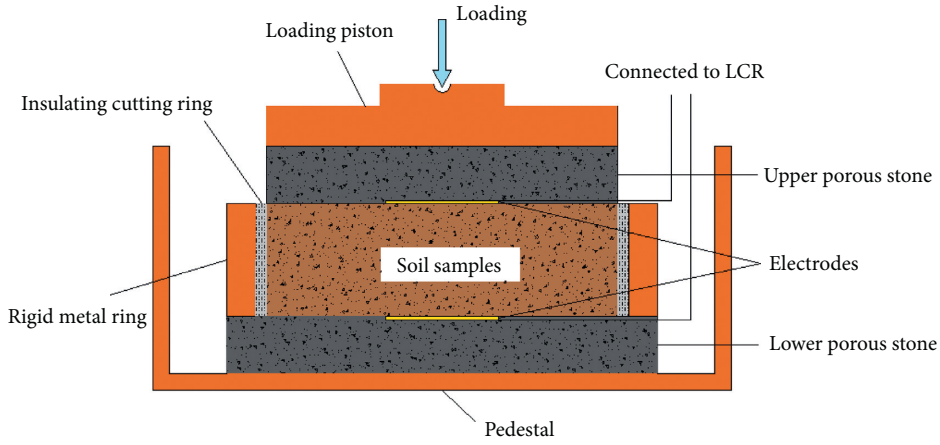


Figure 3: Schematic diagram of the developed consolidation apparatus.

methods of soils for highway engineering [43]. Uniaxial cyclic unloading-reloading tests were conducted to investigate the electrical resistivity and damage properties of compacted loess specimens. First, the loess specimen was loaded at an axial strain rate of 0.5 mm/min until the axial strain reached 0.5%, and it was then unloaded at the same strain rate until the stress decreased to zero. Second, the soil specimen was reloaded up to the second peak strain of 1% at the same strain rate. A 90 s period without any loading between unloading and loading was observed to fully eliminate the effect of loading on the next loading. Such unloading and reloading form a full unloading-reloading cycle. This cycle was repeated, and the other designed peak stains were 1.5%, 2.0%, and 2.5%, respectively, in the subsequent three cycles. During the loading and unloading processes, the stress, strain, and resistivity values were recorded simultaneously.

*2.3.3. DW Cycle Test.* After sample preparation, the individual loess specimen was air-dried at room temperature from an initial water content of 13% to a water content of 1%. Subsequently, a burette was used to gradually add distilled water up to a saturated water content of 18%. Finally, the loess specimens were air-dried at room temperature to an optimum water content of 13%. Subsequently, the specimens were wrapped with plastic films for a period of at least 24 h to achieve a uniform moisture distribution. This drying and wetting procedure is a full DW cycle test. The design DW cycle times in this study were 1, 3, 5, 7, and 10. When the designed DW cycles were achieved, an unconfined compression test or consolidation test was performed on the soil specimens. Note that three to four loess specimens were used for each test (i.e., consolidation tests, unconfined compression test, uniaxial cyclic unloading-reloading tests, and DW cycle test) for replication purposes.

## 3. Results and Discussion

*3.1. Relationship between Electrical Resistivity and Compression Characteristics of Compacted Loess.* The relationship between the electrical resistivity of compacted loess specimens and loading time during the consolidation test is plotted in Figure 4. The electrical resistivity of soil samples exhibited a trend of decreasing abruptly and then gradually becoming constant with each new first load applied. Both the abrupt change in the electrical resistivity and the decreasing range of the consolidation stage were relatively large for loads from 0 to 200 kPa. When the applied load was higher 200 kPa, the electrical resistivity of the loess specimens decreased gradually. In contrast, the vertical compression strain increased with increasing load, and it changed noticeably at the beginning stage (loads less than 200 kPa) and then tended to be constant (Figure 5). Please note that the electrical resistivity changed slightly with a further increase in load and deformation when the load was greater than 200 kPa. This indicated that compression causes the redistribution of water, air, and soil particles in the soil. When the load is small, the compression has a significant effect on the soil structure, which results in a rapid decrease in the electrical resistivity of the soil specimens. As the applied load increases, air is squeezed out of the soil and saturation increases, and the electrical resistivity gradually tends to be constant and becomes less sensitive to changes in stress and strain.

To further explain the relationship between the electrical resistivity and compression characteristics of loess, the relationship curves of void ratio, saturation, and resistivity are plotted in Figure 6. Under the condition of optimal water content, the void ratio of the soil decreases gradually, and the saturation increases with the increase in load. Since the electrical resistivities of soil particles and air in pores are significantly higher than those of pore water, the increase in saturation has a significant effect on the electrical resistivity of soil. Meanwhile, compression of internal pores will result in the connection of some unconnected water pores and form a new conductive path. Thus, at the beginning of the consolidation test, with the decrease in the void ratio and the increase in saturation, the electrical resistivity of the loess decreases significantly. When the applied load is greater than 200 kPa, the change rate of both void ratio and saturation decreases rapidly with the increase in load. Hence, the conductivity channel changes slightly, and the electrical resistivity decreases gradually and tends to be stable. In this study, when the void ratio was greater than 0.56, and the saturation was less than 63%, the electrical resistivity of compacted loess was more sensitive to changes in the void ratio and saturation.

*3.2. Relationship between Stress, Strain, and Resistivity of Compacted Loess.* The stress-strain-resistivity curves of loess specimens under the unconfined compression test indicated that the axial stress attains a peak and then abruptly decreases, exhibiting a typical strain-softening behavior, while the electrical resistivity tends to initially decrease and then increase rapidly (Figure 7). According to the trend of the strain-resistivity curves, it can be divided into four stages. In stage I, the electrical resistivity of loess specimens decreases exponentially with the increase in strain, which corresponds to the compression stage in the stress-strain curve. Under a uniaxial load, air in the pores is discharged rapidly, saturation increases, and pore water connects to form a large number of conductive channels; thus, the resistivity decreases rapidly. In stage II, which corresponds to the elastic stage and strengthening stage in the stress-strain curve, the electrical resistivity of loess specimens decreases with the increase in strain, but the rate of decline rapidly decreases. The soil sample becomes denser after the compaction stage, which makes it difficult for the water and air in the pores to be discharged. As a result, forming new conductive channels is difficult, and the resistivity decreases gradually in this stage. In stage III, the loess specimens are destroyed after attaining the peak strength, and the pores gradually expand and connect, but the soil specimens remain intact, and the electrical resistivity increases gradually. The soil specimens attain the residual strength in stage IV, the fractures overlap by the interconnection of the developing microcracks, and the soil structure is completely destroyed. The conductive channels are constantly broken under the uniaxial load, and the electrical resistivity of the loess specimens increases rapidly. A good real-time correspondence between the electrical resistivity and stress-strain of the loess specimens was observed in the uniaxial compression test. However, compared with stages I and IV, the variation amplitude of electrical resistivity in stages II and III is relatively small, which cannot reflect the variation of stress and strain directly. This makes determining the peak strength of loess samples using electrical resistivity difficult.

The logarithm was obtained for the strain in stages II, III, and IV, and a resistivity-strain semilogarithmic curve was plotted to compare with the uniaxial stress-strain curve more directly (Figure 8). Under a uniaxial load, the stress-strain curve had an approximately straight line when the specimen entered the elastic deformation stage from the compaction stage, and the stress increased proportionally with the strain. After the elastic stage, the stress-strain curve gradually deviated from the straight line, and the soil compressed continuously. When the stress attained the yield limit, the specimen was compressed to the densest state. Correspondingly, after entering the elastic stage, the resistivity-strain semilogarithmic curve also presented an approximately straight line, and the resistivity decreased rapidly with the increase in strain. Subsequently, the rate of resistivity decrease was slightly retarded, but the curve still presented an approximate straight line. When the yield limit was attained, the decrease rate of resistivity was retarded, and the electrical resistivity attained the lowest point when the specimen was destroyed. We observed that the resistivity-strain semilogarithmic curve can better reflect the various stages of the stress-strain curve under a uniaxial load. Before the loess specimen was destroyed, the abrupt

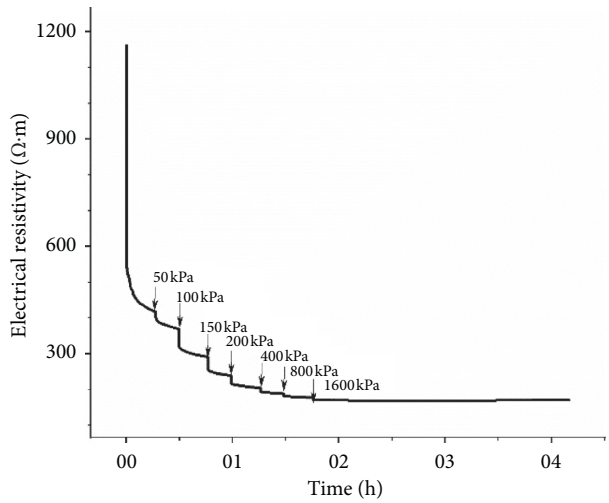


Figure 4: Time-electric resistivity curve in the consolidation test.

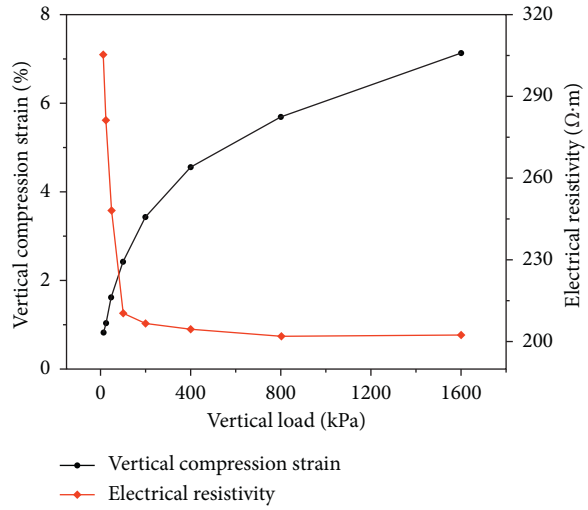


Figure 5: Vertical compression strain-vertical loads-electric resistivity curve of loess.

transition point of the slope of the resistivity-strain semi-logarithmic curve was similar to the yield limit in the stress-strain curve, which may be used as a threshold to determine if the soil sample is about to be destroyed.

*3.3. Relationship between Stress, Strain, and Resistivity of Compacted Loess under the Uniaxial Cyclic Unloading-Reloading Tests.* Figure 9 shows the variation curves of the electrical resistivity and stress of loess specimens over time during the uniaxial cyclic unloading-reloading tests. In the process of axial cyclic loading and unloading, the stress of loess specimens increased and decreased repeatedly, and correspondingly, the electrical resistivity exhibited decreasing and increasing trend. The maximum (minimum) value of stress corresponded to the minimum (maximum) value of electrical resistivity during the test, exhibiting a good corresponding relationship between them. However, the variation amplitudes of resistivity and stress were noticeably different. After each unloading, the stress decreased to 0 kPa, but the electrical resistivity increased slightly and did not increase to the initial value. This indicated that the loading process changed the structure of the loess in that the density increased and the void ratio decreased, and it could not be restored to the original state with unloading.

To explore the relationship between fatigue damage and electrical resistivity of specimens in cyclic loading and unloading tests, the variation in electrical resistivity and stress as a function of strain is shown in Figure 10. For the cyclic behavior, the envelopes of the stress-strain curves were similar to those of the monotonic curves and exhibited a deformation memory of the loess specimen. The shape of the unloading curves was nonlinear and had a concave curvature curve and did not coincide with the loading curve. The loading and unloading curves formed a closed hysteresis loop whose area increased with the increase in loading and unloading times before attaining the failure stress. This

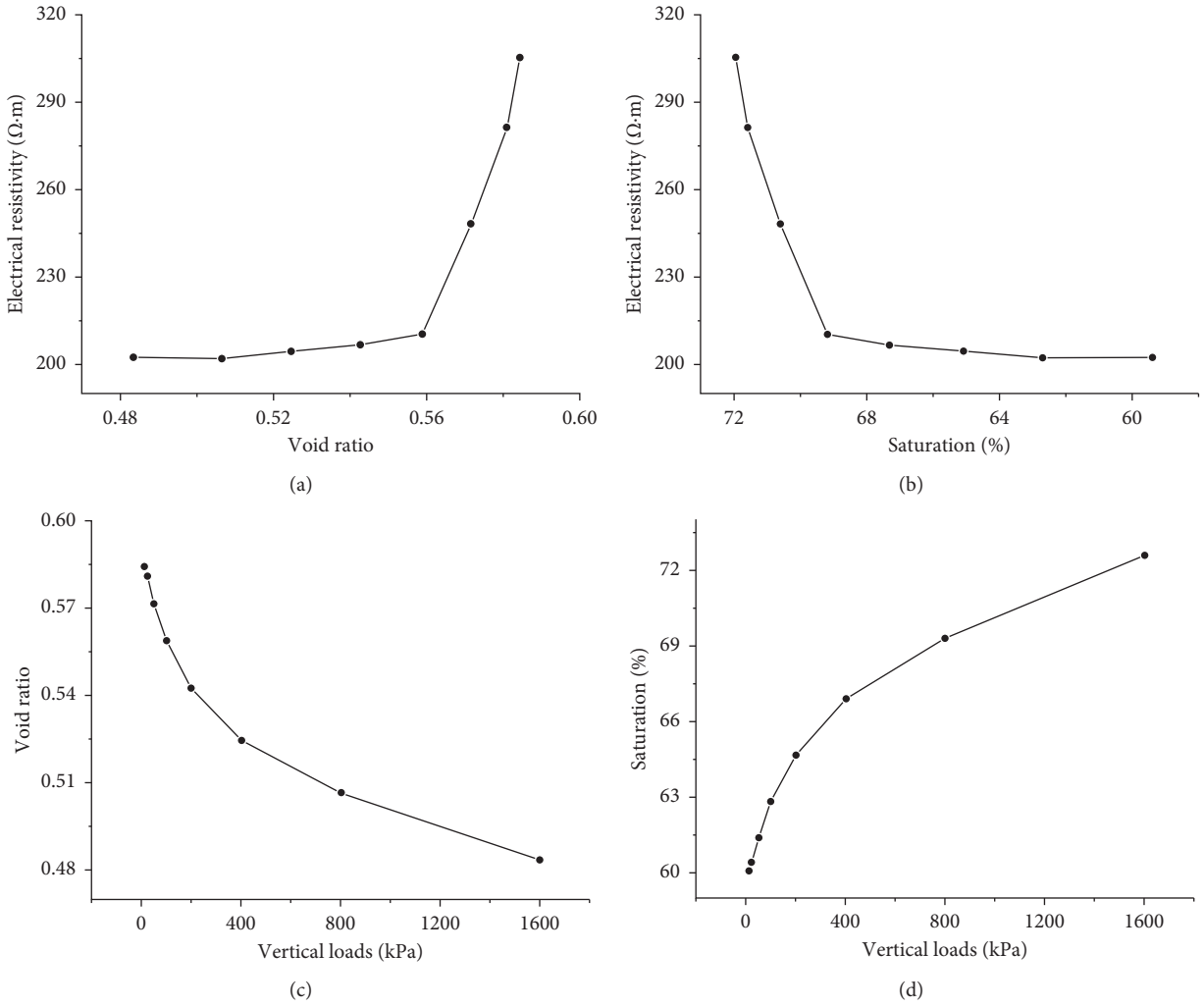


Figure 6: Relationship curve between void ratio, degree of saturation, resistivity, and vertical pressure stress of loess.

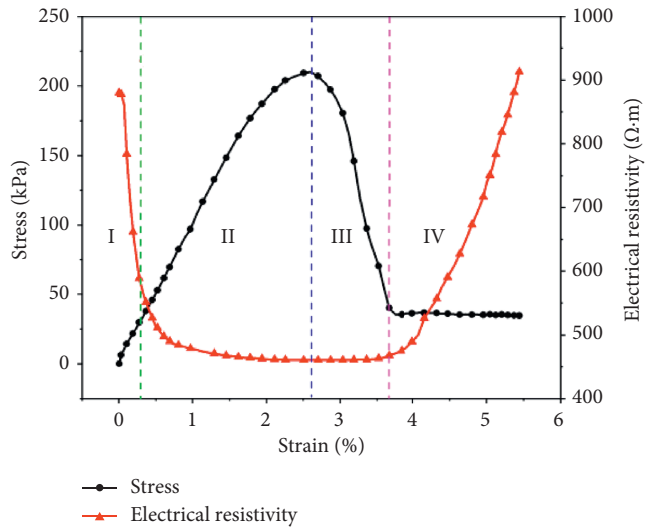


Figure 7: Strain-stress-electric resistivity curve of loess.

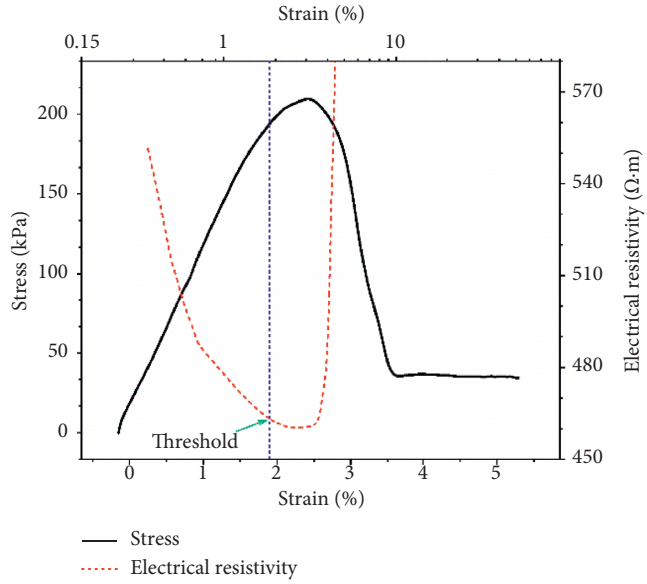


Figure 8: Strain-stress curve and electric resistivity-stress double logarithmic curves of loess.

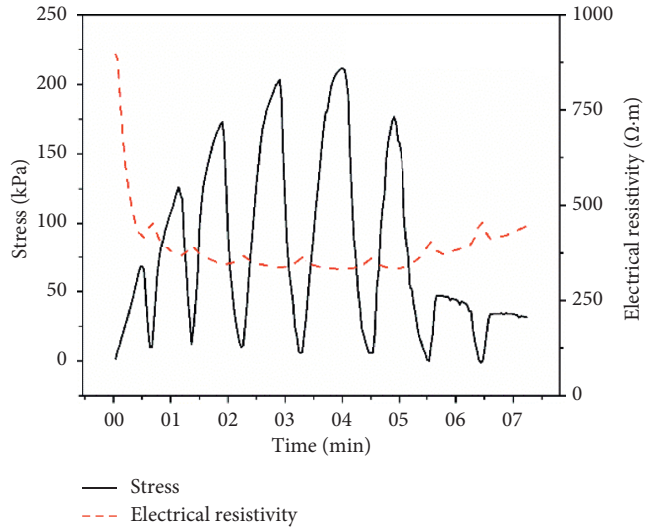


Figure 9: Strain-time-electric resistivity curve of loess under loading and unloading conditions.

indicated that the energy dissipation and fatigue damage of loess specimens increased continuously during loading and unloading [44]. Accordingly, the electrical resistivity curve in Figure 10(b) shows a memory similar to that of the stress-strain curve. The electrical resistivity curves under loading and unloading did not coincide, and closed ring areas were formed before the residual strength was attained. However, as shown in Figure 10(c), the relationship between the area of these rings and the number of unloading-reloading was not apparent. We observed that the electrical resistivity and stress-strain of the specimen had a good correspondence, which can provide a possibility to monitor the engineering properties of loess, which is often subjected to cyclic unloading and reloading. However, there is a certain deficiency in representing the energy dissipation and fatigue damage of the loess under cyclic unloading and reloading.

*3.4. Relationship between Electrical and UCS and Compression Characteristics of Compacted Loess under DW Cycles.* The variations in the vertical compression strain of loess specimens as a function of the load for different DW cycles are shown in Figure 11(a). The vertical compressive strain increased with an increase in the number of DW cycles. Under a load of 1600 kPa, as shown in Figure 11(c), a large increase in the vertical compression strain occurred in the first three DW cycles, followed by a gradual decreased growth rate in additional DW cycles as the DW cycles increased. The electrical resistivity under various loads did not exhibit a uniform monotonous trend with the number of DW cycles. The initial resistivity (without load) of the soil samples increased almost linearly from 374.72 to 508.12 Ω·m as the number of DW cycles increased (Figure 11(d)). After the load was applied, the soil electrical resistivity decreased rapidly as the load increased

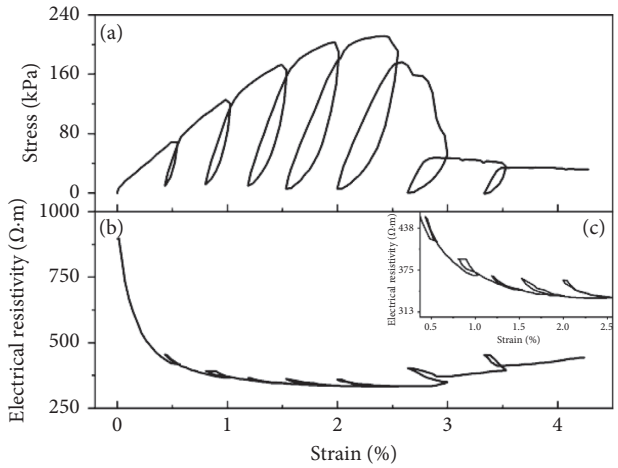


Figure 10: Strain-stress-electric resistivity curve of loess under loading and unloading conditions (Figure 10(c) is a detailed view of Figure 10(b)).

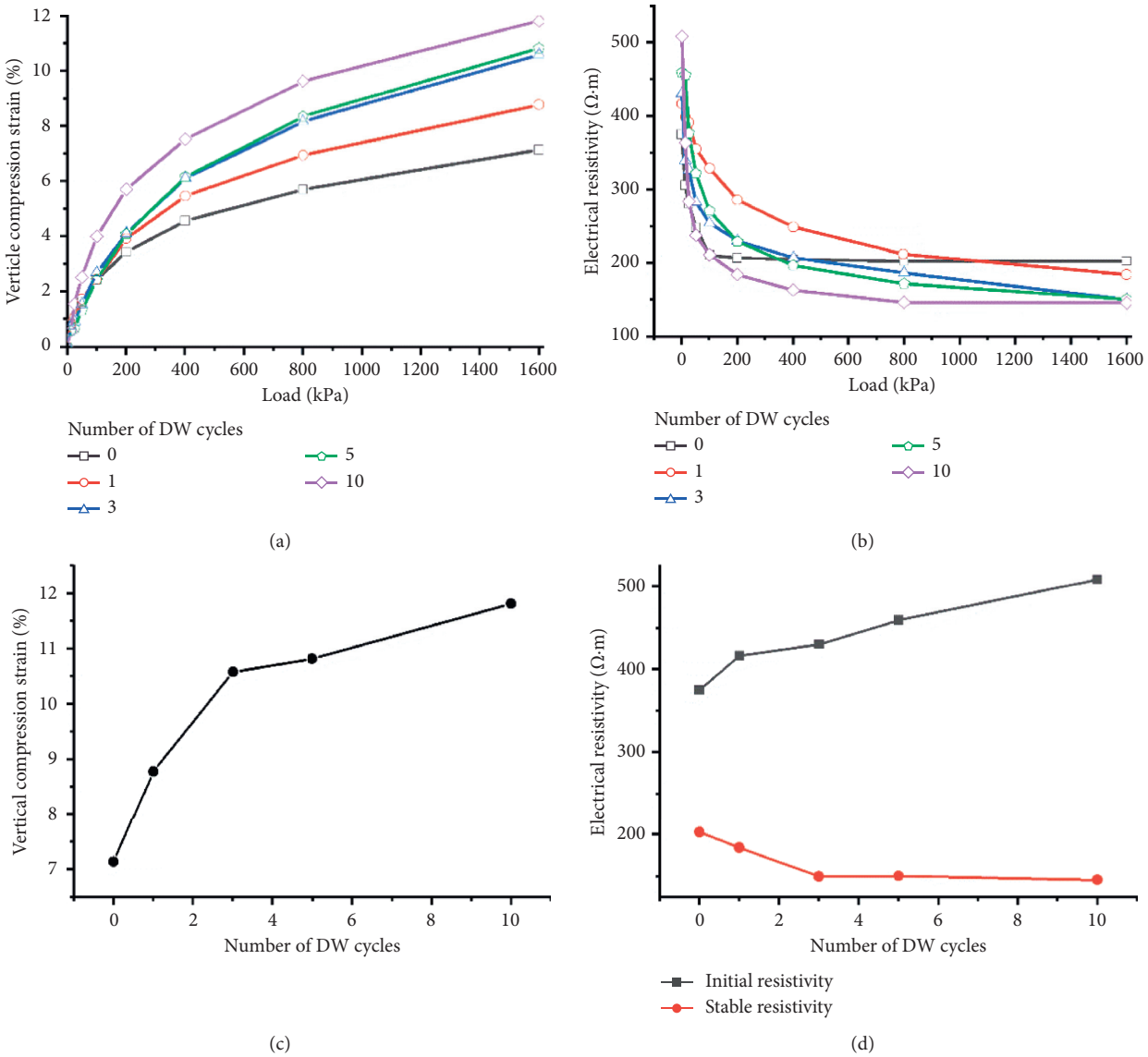


Figure 11: Deformation and electrical resistivity characteristics of loess specimens under different loads and DW cycles: (a) relationship between vertical compression strain and loads under different DW cycles; (b) relationship between electrical resistivity and loads under different DW cycles; (c) relationship between vertical compression strain and DW cycle numbers; (d) relationship between electrical resistivity and DW cycle numbers.

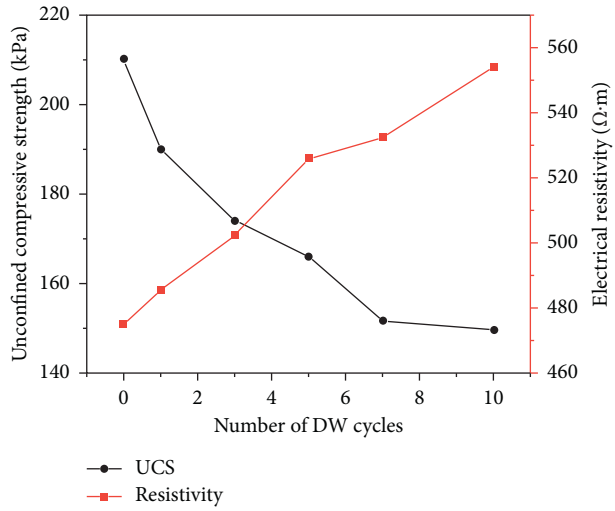


Figure 12: Relationship between UCS, number of DW cycles, and electric resistivity of loess.

(Figure 11(b)). Under a load of 1600 kPa, the electrical resistivity decreased rapidly with an increasing number of DW cycles during the first three DW cycles and then remained constant. The UCS of the loess specimens was also significantly affected by the DW cycles (Figure 12). During the first seven DW cycles, the UCS of loess specimens decreased rapidly with the increase in the number of DW cycles, which indicated a stronger deterioration effect on the compacted loess specimens. The UCS difference of specimens subjected to seven and ten DW cycles was not significant. In contrast, the resistivity increased almost linearly with the number of cycles.

During DW cycles, swelling upon wetting and uneven shrinkage and fissures evolution upon drying would change the soil fabric, rearrange the loess particles, and destroy the integrity of lateritic soil. Thus, a further decrease in strength and increase in deformation of compacted loess are caused by the repeated DW cycles. The changes in the loess inner structure will affect the electrical conductivity of the specimens. The elevated values of electrical resistivity resulting from macrocracking owing to the insulating nature of air impeded current flow. This observation implies that the presence of desiccation cracks in the loess can be identified, which provides the possibility for long-term monitoring of geotechnical properties in the field. However, for consolidation load, the electrical resistivity of the specimens decreased with an increase in the number of DW cycles. The DW cycles cause a more porous and loose structure of the soil, which provides more conductive channels. Before the load is applied, these channels are blocked by air, resulting in high resistivity. As the load increases, the air is squeezed out, and the pore water is connected. Therefore, after the dry and wet cycling and soil compaction, the soil will have a denser structure and lower electrical resistivity. This proves that prewetting can improve the engineering properties of loess and provides a new method for testing the effect of prewetting by using resistivity. However, the strength, deformation, and electrical resistivity of loess specimens subjected to different DW cycles were compared based on the same water content in this study. Considering the significant effect of moisture content on soil electrical resistance [45, 46], the field monitoring based on the electrical resistivity method needs the cooperation of moisture probe, and further study is required.

## 4. Conclusions

In this study, consolidation tests, unconfined compression tests, uniaxial cyclic unloading-reloading tests, and DW cycle tests on densely compacted loess specimens were conducted to assess their deterioration effects on the electrical resistivity and geotechnical properties of compacted loess. The following conclusions can be drawn based on these laboratory results:

(1) Under each load level in consolidation tests, the resistivity of the loess exhibits a tendency of first changing abruptly and then decreasing. The vertical compression strain increases as the vertical load increases, and the change is initially rapid and subsequently slow, which is in contrast to the trend of electrical resistivity. When the load is lower than 200 kPa, the loess resistivity is more sensitive to the load action, while when the load level is higher than 200 kPa, with a further increase in load and deformation, the rate of change of the void ratio and saturation of soil retards, and the resistivity gradually tends to be stable.

(2) During uniaxial compression of loess, the variation in resistivity is closely related to that of stress and strain, which can be divided into four stages: Stage I is the compaction stage, and the resistivity decreases rapidly with the increase in strain. The second stage corresponds to the elastic stage and the plastic failure stage. The resistivity continues to decrease with increasing strain, but the decreasing speed of the resistivity gradually is slower. In stage III, the soil specimen is damaged and attains peak strength, and

the resistivity increases gradually. In stage IV, the soil attains residual strength, the structure is completely destroyed, and the resistivity increases rapidly.

(3) For each unloading-reloading cycle, the electrical resistivity exhibits a trend of initially increasing and then decreasing, and its minimum (maximum) value corresponds to the maximum (minimum) value of the stress. Before soil is destroyed, the maximum value of resistivity after each unloading is smaller than the maximum value of the last unloading, which reflects the irreversible plastic damage caused by soil during loading and unloading. However, a certain deficiency occurs in representing the energy dissipation and fatigue damage of the loess under cyclic unloading and reloading.

(4) The electrical resistivity of loess samples increases as the number of DW cycles increases but decreases with increasing cycle numbers after stabilization under consolidation load. In the unconfined compression test, the UCS of loess specimens decreased rapidly as the number of DW cycles increased during the first seven DW cycles and then remained constant, while the resistivity increased almost linearly with the number of cycles.

(5) The electrical resistivity can effectively characterize the mechanical and deformation characteristics of loess samples under the loads and DW cycles, exhibiting a certain potential for long-term monitoring of soil engineering properties. However, the variation in electrical resistivity is affected by many factors such as water content, temperature, and stress state. Therefore, the effect of the inner structure on electrical resistivity may be much more complex, and further study is required.

## Data Availability

The data used to support the findings of this study are available from the corresponding author upon request.

## Conflicts of Interest

The authors declare that there are no conflicts of interest regarding the publication of this paper.

## Acknowledgments

This work was funded by China's Second Tibetan Plateau Scientific Expedition and Research (2019QZKK0905), the National Natural Science Foundation of China (U1703244 and 41702333), the Science and Technology Major Project of Gansu Province (143GKDA007), and the Research Project of the State Key Laboratory of Frozen Soils Engineering (SKLFSE-ZY-20).

## References

[1] Y. Li, W. Shi, A. Aydin, M. A. Beroya-Eitner, and G. Gao, "Loess genesis and worldwide distribution," *Earth-Science Reviews*, vol. 201, Article ID 102947, 2020.

[2] J. Zhuang, J. Peng, G. Wang, I. Javed, Y. Wang, and W. Li, "Distribution and characteristics of landslide in Loess Plateau: a case study in Shaanxi province," *Engineering Geology*, vol. 236, pp. 89–96, 2018.

[3] D. Liu, *Loess and the Environment*, China Ocean Press, Beijing, China, 1985.

[4] G. Li, F. Wang, W. Ma et al., "Variations in strength and deformation of compacted loess exposed to wetting-drying and freeze-thaw cycles," *Cold Regions Science and Technology*, vol. 151, pp. 159–167, 2018.

[5] W.-L. Xie, P. Li, M.-S. Zhang, T.-E. Cheng, and Y. Wang, "Collapse behavior and microstructural evolution of loess soils from the Loess Plateau of China," *Journal of Mountain Science*, vol. 15, no. 8, pp. 1642–1657, 2018.

[6] Y. Shi, Y. Shen, D. Li et al., *An Assessment of the Issues of Climatic Shift from Warm-Dry to Warm-Wet in Northwest China*, China Meteorological Press, Beijing, China, 2003.

[7] W. K. Ni, K. Z. Yuan, X. F. Lv et al., "Comparison and quantitative analysis of microstructure parameters between original loess and remoulded loess under different wetting-drying cycles," *Scientific Reports*, vol. 10, no. 1, p. 5547, 2020.

[8] H. Lu, J. Li, W. Wang, and C. Wang, "Cracking and water seepage of xiashu loess used as landfill cover under wetting-drying cycles," *Environmental Earth Sciences*, vol. 74, no. 11, pp. 7441–7450, 2015.

[9] C.-m. Hu, Y.-l. Yuan, Y. Mei, X.-y. Wang, and Z. Liu, "Comprehensive strength deterioration model of compacted loess exposed to drying-wetting cycles," *Bulletin of Engineering Geology and the Environment*, vol. 79, no. 1, pp. 383–398, 2020.

[10] Z. H. Yuan, W. K. Ni, C. Tang et al., "Experimental study of structure strength and strength attenuation of loess under wetting-drying cycle," *Rock and Soil Mechanics*, vol. 38, no. 7, pp. 1894–0902, 2017.

[11] Z. Lu, R. Fang, L. Chen et al., "Long-term deformation of highway subgrade under coupling effect of traffic load and drying-wetting cycles," *International Journal of Geomechanics*, vol. 20, no. 2, Article ID 04019168, 2020.

[12] D. Xiao, H. Ma, S. Zhao et al., "Research on pore water pressure and moisture content in soil subjected to freeze-thaw cycles and loading action by model test," *Chinese Journal of Rock Mechanics and Engineering*, vol. 36, no. 4, pp. 977–986, 2017.

[13] J. Chen, S. Wang, J. Zhang et al., "Formation and mechanism of high subgrade diseases of Qinghai-Tibet highway," *Journal of Chang'an University (Natural Science Edition)*, vol. 28, no. 6, pp. 30–35, 2008.

[14] M. Chai, Y. Mu, J. Zhang et al., "Characteristics of asphalt pavement damage in degrading permafrost regions: case study of the Qinghai-Tibet highway, China," *Journal of Cold Regions Engineering*, vol. 32, no. 2, Article ID 05018003, 2018.

[15] G. S. Dasog and G. B. Shashidhara, "Dimension and volume of cracks in a vertisol under different crop covers," *Soil Science*, vol. 156, no. 6, pp. 424–428, 1993.

[16] D. G. Toll, S. D. N. Lourenço, J. Mendes et al., "Soil suction monitoring for landslides and slopes," *Quarterly Journal of Engineering Geology and Hydrogeology*, vol. 44, no. 1, pp. 23–33, 2011.

[17] S. Lee, J. Suh, and H.-d. Park, "Smart compass-clinometer: a smartphone application for easy and rapid geological site investigation," *Computers & Geosciences*, vol. 61, pp. 32–42, 2013.

[18] M. Dyer, S. Utili, and M. Zielinski, "Field survey of desiccation fissuring of flood embankments," *Proceedings of the*

*Institution of Civil Engineers - Water Management*, vol. 162, no. 3, pp. 221–232, 2009.

[19] D. Li, Z. Wu, J. Fang, Y. Li, and N. Lu, "Heat stability analysis of embankment on the degrading permafrost district in the east of the Tibetan Plateau, China," *Cold Regions Science and Technology*, vol. 28, no. 3, pp. 183–188, 1998.

[20] S. Wang, L. Jin, H. Peng, J. Chen, and K. Mu, "Damage analysis of the characteristics and development process of thermosyphon embankment along the Qinghai-Tibet highway," *Cold Regions Science and Technology*, vol. 142, pp. 118–131, 2017.

[21] T. Carlà, E. Intrieri, F. Raspini et al., "Perspectives on the prediction of catastrophic slope failures from satellite InSAR," *Scientific Reports*, vol. 9, no. 1, p. 14137, 2019.

[22] S. Wang, Z. Ahmed, M. Z. Hashmi, and W. Pengyu, "Cliff face rock slope stability analysis based on unmanned arial vehicle (UAV) photogrammetry," *Geomechanics and Geophysics for Geo-Energy and Geo-Resources*, vol. 5, no. 4, pp. 333–344, 2019.

[23] L. D. Jones, "Monitoring landslides in hazardous terrain using terrestrial LiDAR: an example from montserrat," *Quarterly Journal of Engineering Geology and Hydrogeology*, vol. 39, no. 4, pp. 371–373, 2006.

[24] G. E. Archie, "The electrical resistivity log as an aid in determining some reservoir characteristics," *Transactions of the AIME*, vol. 146, no. 01, pp. 54–62, 1942.

[25] K. Arulanandan and K. K. Muraleetharan, "Level ground soil-liquefaction analysis using in situ properties: I," *Journal of Geotechnical Engineering*, vol. 114, no. 7, pp. 753–770, 1988.

[26] S. Y. Liu, Y. J. Du, L. H. Han, and M. F. Gu, "Experimental study on the electrical resistivity of soil-cement admixtures," *Environmental Geology*, vol. 54, no. 6, pp. 1227–1233, 2008.

[27] G. J. Cai, S. Y. Liu, G. H. Shao et al., "Analysis of formation characteristics of marine clay based on resistivity cone penetration test (RCPT)," *Chinese Journal of Geotechnical Engineering*, vol. 30, no. 4, p. 529, 2008.

[28] F. S. Zha, S. Y. Liu, Y. J. Du et al., "The electrical resistivity characteristics of unsaturated clayey soil," *Rock and Soil Mechanics*, vol. 28, no. 8, pp. 1671–1676, 2007.

[29] W. Duan, G. J. Cai, S. Y. Liu et al., "Determining method of cohesionless soil state parameter based on resistivity CPTU and liquefaction evaluation," *Journal of Traffic and Transportation Engineering*, vol. 19, no. 2, pp. 59–68, 2019.

[30] G. J. Cai, T. Zhang, S. Y. Liu et al., "Relationship between electrical resistivity and geotechnical characteristic parameters for Jiangsu marine clay," *Chinese Journal of Geotechnical Engineering*, vol. 35, no. 8, pp. 1470–1477, 2013.

[31] X. Dong, H. Woo, H. Park, and J. Park, "Application of a newly developed column test device to analyze seawater transport in sandy soils," *Environmental Earth Sciences*, vol. 70, no. 5, pp. 2397–2404, 2013.

[32] J. A. Muñoz-Castelblanco, J. M. Pereira, P. Delage et al., "The influence of changes in water content on the electrical resistivity of a natural unsaturated loess," *Geotechnical Testing Journal*, vol. 35, no. 1, pp. 11–17, 2012.

[33] S. Seladji, P. Cosenza, A. Tabbagh, J. Ranger, and G. Richard, "The effect of compaction on soil electrical resistivity: a laboratory investigation," *European Journal of Soil Science*, vol. 61, no. 6, pp. 1043–1055, 2010.

[34] G. Kibria and M. S. Hossain, "Investigation of geotechnical parameters affecting electrical resistivity of compacted clays," *Journal of Geotechnical and Geoenvironmental Engineering*, vol. 138, no. 12, pp. 1520–1529, 2012.

[35] V. A. Rinaldi and G. A. Cuestas, "Ohmic conductivity of a compacted silty clay," *Journal of Geotechnical and Geoenvironmental Engineering*, vol. 128, no. 10, pp. 824–835, 2002.

[36] Z. Liu, Y. Zhang, W. Fang et al., "Experimental research on relationship between electrical resistivity and compactibility of loess," *Journal of Xi'an University of Science and Technology*, vol. 33, no. 1, pp. 84–90, 2013.

[37] M. Long, S. Donohue, J.-S. L'Heureux et al., "Relationship between electrical resistivity and basic geotechnical parameters for marine clays," *Canadian Geotechnical Journal*, vol. 49, no. 10, pp. 1158–1168, 2012.

[38] Ministry of Transport of the People's Republic of China (MCPRC), *Code for Building Construction in Collapsible Loess Regions, GB 50025-2004*, Architecture and Building Press, Beijing, China, 2004.

[39] X. Q. Dong, F. F. Hang, N. N. Su et al., "Experimental study of AC electrical resistivity of unsaturated loess during compression," *Chinese Journal of Rock Mechanics and Engineering*, vol. 34, no. 1, pp. 189–197, 2015.

[40] P. Qin, Y. Liu, Z. Song et al., "An electrical resistivity method of characterizing hydromechanical and structural properties of compacted loess during constant rate of strain compression," *Sensors*, vol. 20, no. 17, p. 4783, 2020.

[41] S. P. Friedman, "Soil properties influencing apparent electrical conductivity: a review," *Computers and Electronics in Agriculture*, vol. 46, no. 1-3, pp. 45–70, 2005.

[42] F. S. Zha, S. Y. Liu, Y. J. Du et al., "Characteristics of electrical resistivity of complacted loess," *Rock and Soil Mechanics*, vol. 32, no. S2, pp. 155–158, 2011.

[43] Ministry of Transport of the People's Republic of China (MTPRC), *Test Methods of Soils for Highway Engineering, JTG E40-2007*, China Communications Press, Beijing, China, 2007.

[44] Y. L. Wei, C. H. Yang, Y. T. Guo et al., "Experimental investigation on deformation and fracture characteristics of brittle shale with natural cracks under uniaxial cyclic loading," *Rock and Soil Mechanics*, vol. 36, no. 6, pp. 1649–1658, 2015.

[45] R. M. Hen-Jones, P. N. Hughes, R. A. Stirling et al., "Seasonal effects on geophysical-geotechnical relationships and their implications for electrical resistivity tomography monitoring of slopes," *Acta Geotechnica*, vol. 12, no. 5, pp. 1159–1173, 2017.

[46] C.-S. Tang, D.-Y. Wang, C. Zhu, Q.-Y. Zhou, S.-K. Xu, and B. Shi, "Characterizing drying-induced clayey soil desiccation cracking process using electrical resistivity method," *Applied Clay Science*, vol. 152, pp. 101–112, 2018.